Explosive synchronization in phase-frustrated multiplex networks

Pitambar Khanra,[1] Prosenjit Kundu,[1] Chittaranjan Hens,[2] and Pinaki Pal[1]
[1]*Department of Mathematics, National Institute of Technology, Durgapur 713209, India*
[2]*Physics and Applied Mathematics Unit, Indian Statistical Institute, Kolkata 700108, India*

(Received 13 August 2018; published 28 November 2018)

We investigate the phenomenon of first-order transition [explosive synchronization (ES)] in an adaptively coupled phase-frustrated bilayer multiplex network. We consider Sakaguchi-Kuramoto dynamics over the top of multiplex networks and we establish that ES can emerge in all layers of a multiplex network even when one of the layers may not exhibit ES in the absence of the interlayer connections. We clearly identify the regions of the parameter space in which the multiplexity wins over the frustration parameter and network structure for the emergence of ES. Based on the mean-field analysis around the coherent state and a perturbative approach around the incoherent state we analytically derive the synchronization transition points (backward and forward) of all layers of the multiplex network as well as its monolayer counterpart satisfying a close agreement with the numerical results.

DOI: 10.1103/PhysRevE.98.052315

I. INTRODUCTION

It had been widely accepted that transition to synchronization in networks of coupled oscillators is a continuous process [1–5] until the discovery of the irreversible or discontinuous synchronization transition [6]. Subsequently, a discontinuous or first-order transition to synchronization [also known as explosive synchronization (ES)] has been extensively explored in networks of coupled oscillators [7–10]. The practicality of ES has been tested in acoustical signal transduction in the cochlea (modeling the hair cell) [11], hypersensitivity in fibromyalgic brains [12], and experimentally verified in mercury beating-heart (MBH) oscillators [13]. Researchers reported that ES can be achieved by correlating the natural frequencies with the degrees of the networks [9,14] or by designing a frequency-based weighted coupling [15–17].

However, these preconditions for the emergence of ES in a network of oscillators can be waived by setting an adaptive factor in the coupling term where adaptation is extracted from the global order parameter of the phase oscillators [18]. Recently, the adaptive strategy has also been extended in complex networks (including multiplex networks) of phase oscillators [19,20], where it has been shown that a partial fraction of nodes controlled by their adaptively coupled local order parameter can induce ES in a network of Kuramoto dynamics for arbitrary frequency distribution. The strategy has been found to be general in nature and tested in multiplex networks irrespective of the diversion of frequency distributions between the layers. The growing interest among the researchers to investigate dynamical processes in multiplex networks [21,22] may be attributed to the fact that diverse complex systems ranging from engineering to transportation or to ecology can be mapped to multiplex networks [23]. Moreover, due to the presence of layer-layer interaction in multiplex networks, some nontrivial effect on different dynamical phenomena is expected. For instance, the role of layer-layer interaction in multiplex networks on the dynamical process of diffusion [24] can be faster in multiplex network than its monolayer counterpart due to layer-layer interaction.

Here we have focused on an adaptively coupled phase-frustrated multiplex network, expecting that the presence of layer-layer interaction may induce unexpected effect on the synchronization transition. We have considered either (1) each layer is structurally different than the other, i.e., heterogeneity of the degree distributions are not identical although both layers consist of the same dynamics (identical frustration and frequencies are drawn from the same distribution), or (2) both the networks are structurally equivalent but dynamically different (frustration terms are not identical). Note that for both cases, one of the layers shows continuous transition in the absence of interlayer interaction.

The key question we ask here is whether ES can be established in all layers of a multiplex network in which one of the layers may not exhibit ES in the absence of interlayer connections. We have tried to answer the question by exploring a multiplexed (bilayer) phase-frustrated system [25] called Sakaguchi-Kuramoto (SK) dynamics. We have shown that an adaptive multiplex network can indeed exhibit ES in all phase-frustrated layers. More precisely our paper establishes that fact (with proper analytical treatment) that depending on the network structure and frustration parameter, a monolayer may not exhibit ES but it does guarantee ES in a multilayer structure if at least one of its layers is in the regime of ES, an interesting phenomena not explored earlier in frustrated environments. To validate our numerical results we have used an annealed network based approximation [26–28] to construct coupled equations of order parameter and group angular velocity. The backward transition point is numerically calculated from these two coupled equations. We have also used perturbative approach around the incoherent state [29] to find the forward transition point of the hysteresis loop.

We consider two complex networks of same size N which form a multiplex network if there are intralayer connections. A schematic diagram of a multiplex network in the presence of a special type of intralayer connection is shown in Fig. 1. Thick black lines (shown in two surfaces) represent intralayer interaction and layer-layer interaction (interlayer) is described by the dashed lines. Note that the connectivity between layer I

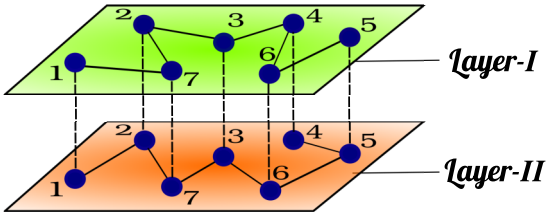

FIG. 1. Schematic diagram of a multiplex network consisting of two layers of different network topologies.

and layer II is chosen in such a way that coupled pairs of nodes have the same index; i.e., node 1 of layer I will be connected to node 1 of layer II and so on. The layers are controlled by cross adaptive feedback [19] to each other through the interlayer (dashed lines) interaction.

The phase $\theta_{i,\sigma(t)}$ of the ith oscillator ($i = 1, \ldots, N$) of the layer σ (= I, II) is evolved by the differential equation

$$\frac{d\theta_{i,\sigma}}{dt} = \omega_{i,\sigma} + \lambda f_{i,\sigma} \sum_{j=1}^{N} A_{ij}^{\sigma} \sin(\theta_{j,\sigma} - \theta_{i,\sigma} - \alpha), \quad (1)$$

where $(A_{ij}^{\sigma})_{N\times N}$ and $\omega_{i,\sigma}$ respectively denote the adjacency matrix and natural frequency of the ith oscillator of the layer σ (= I, II), while λ and α denote the uniform coupling strength and phase-lag parameters, respectively. The parameter $f_{i,\sigma} = r_{i,\sigma'}$ or $r_{i,\sigma}$ according to whether there is an interlayer connection or not, where $\sigma' =$ I, II and $\sigma \neq \sigma'$; i.e., if $\sigma =$ I, then $\sigma' =$ II and vice versa. The local order parameter $r_{i,\sigma}$ of the layer σ (= I, II) is defined by $r_{i,\sigma}e^{i\phi_{\sigma}} = (1/k_{i,\sigma})\sum_{j=1}^{N} A_{ij}^{\sigma} e^{i\theta_{j,\sigma}}$, where $k_{i,\sigma}$ and ϕ_{σ} are the degree of ith node and average local phase of the layer σ (= I, II). Now $R_{\sigma}e^{i\psi_{\sigma}} = (1/N)\sum_{j=1}^{N} e^{i\theta_{j,\sigma}}$ describes the global order parameter of the layer σ with $0 \leqslant R_{\sigma} \leqslant 1$ and average phase ψ_{σ}.

II. NUMERICAL SIMULATION IN MULTIPLEX NETWORK

At the outset, we take an Erdös-Rényi (ER) network of size $N = 2000$, mean degree $\langle k\rangle \sim 12$ in layer I and a heterogeneous scale-free (SF) network of the same size ($N = 2000$), scaling exponent $\gamma = 2.5$, and mean degree $\langle k\rangle \sim 16$ in the second layer (II) in absence of interlayer interaction. In this case, the layers are separated and controlled by their self local order feedback ($f_{i,\sigma} = r_{i,\sigma}, i = 1, 2, \ldots, N$). The natural frequencies of both the layers ($\omega_{i,\sigma}; \sigma =$ I, II) are drawn from a random homogeneous distribution spread over the range -1 to 1. We now numerically integrate the system (1) using a fourth-order Runge-Kutta scheme (RK4). For forward (backward) continuation we adiabatically increase (decrease) the coupling strength λ with an increment (decrement) of $\delta\lambda = 0.01$. The adaptively coupled ER network in layer I is found to exhibit ES in the presence of weak frustration [see Fig. 2(a)]. The frustration parameter has no impact on the forward critical point λ_f where the ensemble transits from incoherence to coherence during forward continuation. The λ_f for all α is shown by the black arrow in Fig. 2(a). However, during backward continuation, the critical point λ_b of transition from coherence to incoherence is found to move towards higher λ

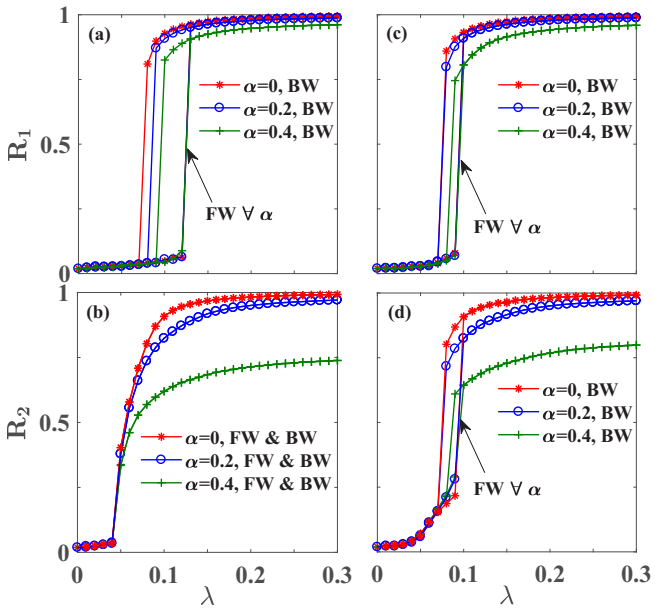

FIG. 2. Global order parameters of two layers as a function of coupling parameter λ for different values of α. Synchronization transitions in different layers in the absence of interlayer interactions are shown in panels (a) and (b), while those in the presence of interlayer interactions are shown in (c) and (d) for three different values of α.

as α is increased and as a result, the width of hysteresis loop decreases. Next the transition is examined in layer II (SF) in the absence of interlayer interaction. The frustrated dynamics used on top of the scale-free network ($\gamma = 2.5$ and $\langle k\rangle \sim 16$) does not exhibit ES [see Fig. 2(b)], although the transition looks like a hybrid [26], or the ES, if it exists, is negligibly small [20]. The critical transition point for the onset of the second-order/continuous phase transition is also independent of α; a peculiar but generic behavior is found to occur for all types of adaptive networks.

Now we connect both the layers with cross-adaptive interlayer interaction ($f_{i,\sigma} = r_{i,\sigma'}, i = 1, 2, \ldots, N$) and we observe that ES is fully established in both the layers. The transition points and hysteresis loops are clearly shown in Figs. 2(c), 2(d) for layer I and layer II, respectively due to the presence of cross-adaptive feedback, i.e., interlayer interaction. We also observe that forward critical transition points do not depend on the frustration parameter present in the systems although it shrinks the ES width if we increase α. Note that the value of the order parameter of the second layer II is also slightly increased due to the impact of multiplexity. We now present a detailed and rigorous analytical description of these numerically observed results. We start with an analytical treatment of the monolayer counterparts of the multiplex in the absence of interlayer connections.

III. MEAN FIELD ANALYSIS

In the absence of the interlayer connections, the layers of the multiplex are separated. Here we perform the mean-field analysis of the isolated layers of the multiplex following the approach proposed in [27]. Let the density of the nodes at

time t with phase θ for a given degree k and frequency ω be given by the function $\rho(k,\omega,\theta,t)$ with a proper normalization condition

$$\int_0^{2\pi} \rho(k,\omega;\theta,t)d\theta = 1. \tag{2}$$

Avoiding the degree-degree correlation of a network we obtain the probability that a randomly chosen edge attached to a node with degree k and phase θ at time t is

$$\frac{kP(k)g(\omega)\rho(k,\omega;\theta,t)}{\int kP(k)dk}. \tag{3}$$

Then in the continuum limit, time evolution of the phases of the oscillators of a layer is given by

$$\frac{d\theta(t)}{dt} = \omega + \frac{\lambda f k}{\langle k\rangle}\int dk' \int d\omega' \int d\theta' k' P(k')g(\omega') \times \rho(k',\omega',\theta',t)\sin(\theta'-\theta-\alpha), \tag{4}$$

where $\langle k\rangle = \int kP(k)dk$ is the mean degree of the network. To maintain the conservation of the oscillators [4,27] in a layer, the density function ρ satisfies the continuity equation

$$\frac{\partial\rho}{\partial t} + \frac{\partial}{\partial\theta}(\rho v) = 0, \tag{5}$$

where v comes from the right-hand side of Eq. (4).

To measure the macroscopic behavior of the oscillators, in the thermodynamic limit we consider the order parameter R given by [27]

$$Re^{i\psi} = \frac{1}{\langle k\rangle}\int dk \int d\omega \int d\theta k P(k)g(\omega)\rho(k,\omega,\theta,t)e^{i\theta}, \tag{6}$$

where ψ is the average phase of the oscillators and the value of R varies in the range $0 \leqslant R \leqslant 1$. Therefore, inserting (6) into (4) we obtain

$$\frac{d\theta}{dt} = \omega + \lambda r k R\sin(\psi-\theta-\alpha). \tag{7}$$

In our present study we consider $f_i = r_i$ $(i = 1,\ldots,N)$, where r_i is the local order parameter. Now we derive the self-consistent equations by setting the global phase $\psi(t) = \Omega t$, where Ω is the group angular frequency. Further we introduce a new variable ϕ with $\phi(t) = \theta(t) - \psi(t) + \alpha$. In this rotating frame the equation can be written as

$$\frac{d\phi}{dt} = \omega - \Omega - \lambda r k R\sin(\phi). \tag{8}$$

Inserting Eq. (8) into (5) and using the integral expression of order parameter (6) we get the steady state solution of $\rho(k,\omega;\phi)$ by setting $\frac{\partial}{\partial t}\rho(k,\omega,\phi) = 0$. Therefore, the steady state solution for the density function ρ is given by

$$\rho(k,\omega;\phi) = \delta\left(\phi - arc\sin\left(\frac{\omega-\Omega}{\lambda r k R}\right)\right);\ \left|\frac{\omega-\Omega}{\lambda r k R}\right| \leqslant 1 = \frac{A(k,\omega)}{|\omega-\Omega-\lambda r k R\sin(\phi)|};\ \left|\frac{\omega-\Omega}{\lambda r k R}\right| > 1,$$

where δ is the Dirac delta function and $A(k,\omega)$ is the normalization constant. The first solution corresponds to the synchronous state (a locked version) and the second solution is due to the desynchronous state (a drift version). Hence the order parameter can be rewritten as

$$R = \frac{1}{\langle k\rangle}\int\left[\int\int_{k_{min}}^{\infty} kP(k)g(\omega)\rho(k,\omega,\phi) \times e^{i(\phi-\alpha)}H_1 dk d\omega + \int\int_{k_{min}}^{\infty} kP(k)g(\omega) \times \rho(k,\omega,\phi)e^{i(\phi-\alpha)}H_2 dk d\omega\right]d\phi, \tag{9}$$

where $H_1 \approx H(1-|\frac{\omega-\Omega}{\lambda r k R}|)$ and $H_2 \approx H(|\frac{\omega-\Omega}{\lambda r k R}|-1)$. Here H is Heaviside function. Note that the first part of the right-hand side of Eq. (9) gives the contribution of locked oscillators and the second part corresponds to the contribution of drift oscillators to the order parameter R.

Decomposing Eq. (9) (see the Appendix for more detailed calculation) we can eventually reach two coupled equations

$$R\langle k\rangle = \cos\alpha\int\int kP(k)g(\omega)\sqrt{1-\left(\frac{\omega-\Omega}{\lambda r k R}\right)^2}H_1 dk d\omega + \frac{\sin\alpha}{\lambda r R}(\langle\omega\rangle-\Omega) - \sin\alpha\int\int kP(k)g(\omega)\frac{\omega-\Omega}{\lambda r k R}\sqrt{1-\left(\frac{\lambda r k R}{\omega-\Omega}\right)^2}H_2 dk d\omega \tag{10}$$

and

$$\langle\omega\rangle - \Omega = \lambda r R\tan\alpha\int\int kP(k)g(\omega)\sqrt{1-\left(\frac{\omega-\Omega}{\lambda r k R}\right)^2}H_1 dk d\omega + \int\int P(k)g(\omega)(\omega-\Omega)\sqrt{1-\left(\frac{\lambda r k R}{\omega-\Omega}\right)^2}H_2 dk d\omega. \tag{11}$$

These two coupled equations describe the behavior of the macroscopic order parameter (R) and common frequency (Ω) emerged from the coupled network. To solve these coupled equations (10) and (11) we use the information of the network structure (the degree sequences) and the frequency distribution. Note that in the uncorrelated configuration model, the local order parameter behaves similarly to the global order parameter ($r_i \sim R$) in the thermodynamic limit.

Next, we extend the annealed network approximation approach in a multilayer network [Eq. (1)] where each layer is controlled by an adaptive feedback from the other layer. The mathematical formalism leads us to four coupled equations for two layers in which the first two equations contain the information of two global frequencies of two layers whereas the other two equations contain the information of order parameters. Based on Eqs. (10) and (11) we may write

$$\langle\omega_\sigma\rangle - \Omega_\sigma = \lambda r_{\sigma'} R_\sigma \tan\alpha \int\int k_\sigma P(k_\sigma) g(\omega_\sigma) \sqrt{1 - \left(\frac{\omega_\sigma - \Omega_\sigma}{\lambda r_{\sigma'} R_\sigma k_\sigma}\right)^2} H_{1\sigma} dk_\sigma d\omega_\sigma + \int\int P(k_\sigma) g(\omega_\sigma)(\omega_\sigma - \Omega_\sigma) \sqrt{1 - \left(\frac{\lambda r_{\sigma'} R_\sigma k_\sigma}{\omega_\sigma - \Omega_\sigma}\right)^2} H_{2\sigma} dk_\sigma d\omega_\sigma \tag{12}$$

and

$$R_\sigma \langle k_\sigma\rangle = \cos\alpha \int\int k_\sigma P(k_\sigma) g(\omega_\sigma) \sqrt{1 - \left(\frac{\omega_\sigma - \Omega_\sigma}{\lambda r_{\sigma'} R_\sigma k_\sigma}\right)^2} H_{1\sigma} dk_\sigma d\omega_\sigma + \frac{\sin\alpha}{\lambda r_{\sigma'} R_\sigma}(\langle\omega_\sigma\rangle - \Omega_\sigma) - \sin\alpha \int\int k_\sigma P(k_\sigma) g(\omega_\sigma) \frac{\omega_\sigma - \Omega_\sigma}{\lambda r_{\sigma'} R_\sigma k_\sigma} \sqrt{1 - \left(\frac{\lambda r_{\sigma'} R_\sigma k_\sigma}{\omega_\sigma - \Omega_\sigma}\right)^2} H_{2\sigma} dk_\sigma d\omega_\sigma, \tag{13}$$

where $H_{1\sigma} \approx H(1 - |\frac{\omega_\sigma - \Omega_\sigma}{\lambda r_{\sigma'} R_\sigma k_\sigma}|)$, $H_{2\sigma} \approx H(|\frac{\omega_\sigma - \Omega_\sigma}{\lambda r_{\sigma'} R_\sigma k_\sigma}| - 1)$, and $\sigma, \sigma' = \mathrm{I},\ \mathrm{II}\ (\sigma \neq \sigma')$.

Figure 3 shows how the system changes from coherent state to incoherent state as obtained both from numerical simulation of the full system (1) and the self-consistent equations (10)–(13) in the absence of phase frustration ($\alpha = 0$). The red lines display the order parameter obtained from numerical simulation of the full system and blue lines show the order parameter obtained from semianalytical simulation using Eqs. (10) and (11) in Figs. 3(a) and 3(b) in the absence of interlayer interaction, while Figs. 3(c) and 3(d) show the same in the presence of interlayer interaction. Note that in Figs. 3(c) and 3(d), the blue lines are computed from the self-consistent equations (12) and (13). The critical backward transition points are then computed from the extreme left end of the blue curves.

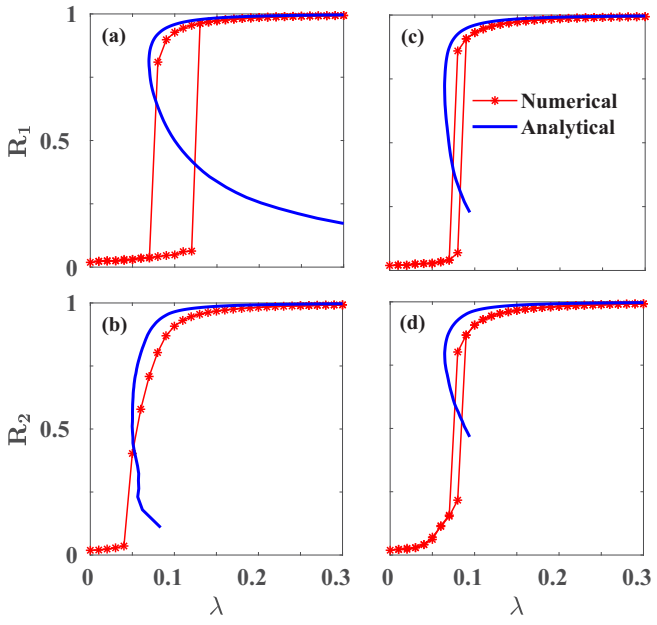

FIG. 3. Comparison of synchronization transition of two layers for the numerical result with the analytical by setting the phase-frustration parameter $\alpha = 0$. The red line indicates the numerical simulation and blue lines are drawn from the coupled equations (10) and (11) for (a) and (b). Equations (12) and (13) are used for panels (c) and (d). The left panels show the synchronization phenomenon in the absence of interlayer interaction and the right panels show the same when the layers are connected through adaptive links.

Now to validate the self-consistent equations rigorously we tune both layers from the nonfrustrated regime ($\alpha = 0$) to the highly frustrated regime ($\alpha \sim 1$) in the absence as well as in the presence of interlayer interactions. In the absence of interlayer interactions, we perform numerical simulation of the networks in both the layers and demarcate the coherent and incoherent regimes in the α-λ plane. Note that in layers I and II we have considered ER and SF networks of size $N = 2000$, respectively. Figures 4(a) and 4(b) show the impact of phase frustration on layers I and II in the absence of interlayer interaction. The cyan island (III) represents the coherent/synchronization regime and the green island (I) shows the incoherent regime. The ES regime is shown by the red island. From Fig. 4(a) we observe that the ER network exhibits ES for a broad range of frustration ($0 < \alpha < 0.75$), whereas the SF network fails to exhibit ES for any value of α [see Fig. 4(b)]. Now we consider interlayer interaction via cross-adaptive feedback between the two layers and interestingly, we observe that the multiplexity helps the emergence of ES in both the layers as is evident from Figs. 4(c) and 4(d). A small red island appears in layer II (SF) signifying the presence of a metastable (ES or hysteresis) state which was missing in its monolayer counterpart. Due to the impact of diffusion, the hysteresis loop (width) is slightly reduced in the ER layer. The black line (upper end of the green island) represents the backward transition (λ_b), i.e., the changes from the coherence state to incoherence state. These numerically computed boundaries have also been validated using the self-consistent coupled equations (10) and (11) for a monolayer and (12) and (13) for multilayers shown with black lines at the upper end of the green island [Figs. 4(a) and 4(b) and Figs. 4(c) and 4(d), respectively]. Note that these critical boundaries for the

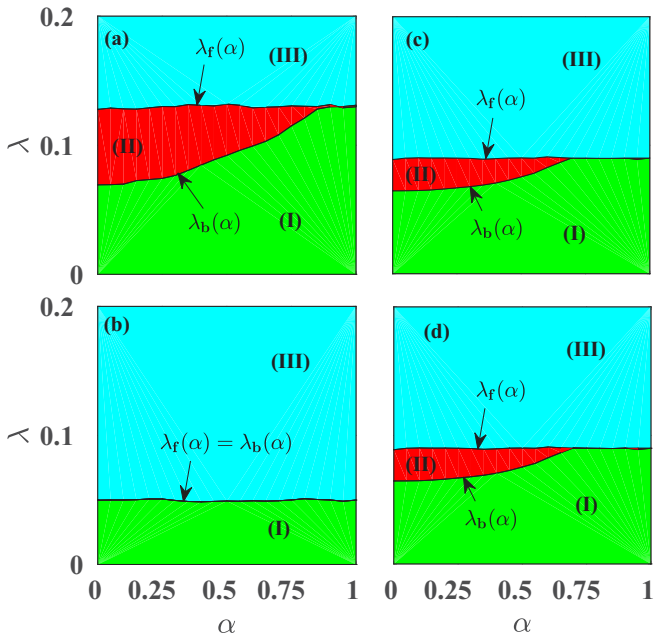

FIG. 4. Phase diagram on α-λ plane showing different regions in two layers of the multiplex in the absence [(a) and (b)] and presence [(c) and (d)] of interlayer interactions. Green (I), red (II), and cyan (III) islands respectively represent asynchronous ($R \sim 0$), hysteresis, and synchronous ($R \sim 1$) regions. These regions are separated by solid black lines indicating the critical coupling strength for the transition to synchrony during the forward (λ_f) and backward (λ_b) continuation.

backward points are computed from the extreme left end points of the curves obtained numerically from the self-consistent equations (10)–(13) for different values of α (e.g., for $\alpha = 0$, backward transition points are computed from the extreme left end points of the blue curves shown in Fig. 3). The mean-field analysis also confirms the existence of the metastable state (ES). However the forward transition point (end of metastable state) cannot be predicted from this analysis, a peculiar issue discussed earlier in [19,20] due to the fluctuation in the order parameter.

In the next section, we derive the exact formula for forward transition point to synchronization analytically.

IV. FORWARD TRANSITION

To determine the exact forward transition point (λ_f) analytically, we proceed by perturbing the completely incoherent state [29]. In the completely incoherent state $\rho(k,\theta,\omega,t) = \frac{1}{2\pi}$ and it is perturbed with small amplitude η as

$$\rho(k,\theta,\omega,t) = \frac{1}{2\pi} + \epsilon\eta(k,\theta,\omega,t), \text{ where } \epsilon \ll 1. \quad (14)$$

Since $\int_o^{2\pi} \eta(k,\theta,\omega,t)d\theta = 0$, we have

$$\begin{aligned} R'e^{i\psi} &= \frac{1}{\langle k\rangle}\int\int\int kP(k)g(\omega)\rho(k,\omega,\theta,t)e^{i\theta}d\theta d\omega dk \\ &= \frac{\epsilon}{\langle k\rangle}\int\int\int kP(k)g(\omega)\eta(k,\omega,\theta,t)e^{i\theta}d\theta d\omega dk \\ &= \epsilon Re^{i\psi}, \end{aligned} \quad (15)$$

which imply $R' = \epsilon R$ and

$$Re^{i\psi} = \frac{1}{\langle k\rangle}\int\int\int kP(k)g(\omega)\eta(k,\omega,\theta,t)e^{i\theta}d\theta d\omega dk. \quad (16)$$

The flow velocity function $v(t)$ is defined by

$$\begin{aligned} v(t) = \frac{d\theta}{dt} &= \omega(t) + \lambda rkR'\sin(\psi-\theta-\alpha) \\ &= \omega(t) + \epsilon\lambda rkR\sin(\psi-\theta-\alpha). \end{aligned} \quad (17)$$

By substituting (14), (16), (17) into (5) and neglecting the higher-order term of ϵ, we have

$$\frac{\partial\eta}{\partial t} = -\omega\frac{\partial\eta}{\partial\theta} + \frac{\lambda rkR\cos(\psi-\theta-\alpha)}{2\pi}. \quad (18)$$

Now the complex Fourier series of the function $\eta(k,\theta,\omega,t)$ is given by

$$\begin{aligned} \eta(k,\theta,\omega,t) &= c(k,\omega,t)e^{i\theta} + c^*(k,\omega,t)e^{-i\theta} \\ &\quad + \eta^{\perp}(k,\theta,\omega,t), \end{aligned} \quad (19)$$

where $\eta^{\perp}$ represents the higher-order Fourier harmonic terms. Now,

$$\begin{aligned} Re^{i(\psi-\theta-\alpha)} = e^{-i(\theta+\alpha)}Re^{i\psi} &= \frac{e^{-i(\theta+\alpha)}}{\langle k\rangle}\int\int\int kP(k)g(\omega) \\ &\quad \times \eta(k,x,\omega,t)e^{ix}d\omega dx dk = \frac{2\pi e^{-i(\theta+\alpha)}}{\langle k\rangle} \\ &\quad \times \int\int kP(k)g(\omega)c^*(k,\omega,t)d\omega dk. \end{aligned} \quad (20)$$

Similarly we can write

$$Re^{-i(\psi-\theta-\alpha)} = \frac{2\pi e^{i(\theta+\alpha)}}{\langle k\rangle}\int\int kP(k)g(\omega)c(k,\omega,t)d\omega dk. \quad (21)$$

Now combining Eq. (20) and Eq. (21) we can get

$$\begin{aligned} &R\cos(\psi-\theta-\alpha) \\ &= \frac{\pi}{\langle k\rangle}\Big[e^{-i(\theta+\alpha)}\int\int kP(k)g(\omega)c^*(k,\omega,t)d\omega dk \\ &\quad + e^{i(\theta+\alpha)}\int\int kP(k)g(\omega)c(k,\omega,t)d\omega dk\Big]. \end{aligned} \quad (22)$$

Using Eqs. (19) and (22) in Eq. (18) and comparing the coefficients of $e^{i\theta}$ we arrive at

$$\begin{aligned} \frac{\partial c(k,\omega,t)}{\partial t} &= -i\omega c(k,\omega,t) + \frac{\lambda rk}{2\langle k\rangle}e^{i\alpha}\int_{k_{min}}^{\infty}\int k'P(k') \\ &\quad \times g(\omega')c(k',\omega',t)d\omega' dk'. \end{aligned} \quad (23)$$

We now assume $c(k,\omega,t) = A(k)B(\omega)e^{\mu t}$ and substituting it into Eq. (23) we get

$$\begin{aligned} \mu A(k)B(\omega) &= -i\omega A(k)B(\omega) + \frac{\lambda rk}{2\langle k\rangle}e^{i\alpha}\int_{k_{min}}^{\infty}\int_{-\infty}^{\infty}k' \\ &\quad \times P(k')g(\omega')A(k')B(\omega')d\omega' dk'. \end{aligned} \quad (24)$$

Finally, the equation looks like

$$1 = \frac{\lambda r \langle k^2 \rangle}{2\langle k \rangle} e^{i\alpha} \int \frac{(\mu - i\omega) g(\omega)}{\mu^2 + \omega^2} d\omega. \tag{25}$$

For symmetric uniform frequency distribution within an interval $[-a, a]$, $g(\omega) = \frac{1}{2a}$ for $-a \leqslant \omega \leqslant a$ and $g(\omega) = 0$, otherwise. In that case, from (25), we get

$$\lambda_f = \frac{4a\langle k \rangle \cos\alpha}{\pi R \langle k^2 \rangle}, \tag{26}$$

by taking the limit $\mu \to 0$ for marginal stability and $r \sim R$ due to the annealed network approximation. Here λ_f gives the forward transition point where the incoherent state loses its stability. The expression of λ_f (26) combines the network structure ($\langle k \rangle$ and $\langle k^2 \rangle$), with the system parameters frequency distribution $g(\omega)$ and the phase-frustration parameter α. Note that the ratio of the first nonzero order parameter (R) and $\cos\alpha$ remains constant for a given network (numerical verification is not shown here); therefore λ_f depends only on network structure and frequency distribution. The approach fits with our numerical result shown in Figs. 2(a) and 2(b) where the forward point does not depend on α. The same behavior is also shown with black lines (lower end of cyan island) in Figs. 4(a) and 4(b). As expected, the black lines are almost parallel to the x axis (α). In the absence of interlayer connection we calculate the forward critical point from (26), in which the values for the layer I and layer II are $\lambda_f \sim 0.12$ and $\lambda_f \sim 0.04$, respectively. We have verified our result for several choices of initial states. Note that the forward transition point of the scale-free layer (II) is close to zero, as we consider $\gamma = 2.5$, where $\frac{\langle k \rangle}{\langle k^2 \rangle}$ converges to zero for $N \to \infty$ as the nodes with higher degree (hubs) enhance the synchronization process [30]. Due to finite network size we get a small nonzero λ_f value. Next we have extended our forward transition calculation in the multilayer network in the presence of interlayer interaction and obtain

$$\lambda_{\sigma_c} = \frac{4a\langle k_\sigma \rangle \cos\alpha}{\pi r_{\sigma'} \langle k_\sigma^2 \rangle}; \quad \sigma, \sigma' = \mathrm{I},\ \mathrm{II}\ (\sigma \neq \sigma'). \tag{27}$$

Due to the diffusive interaction, critical points of both layers remain close to each other; the total hysteresis areas of both layers [shown in red color in Figs. 4(c) and 4(d)] remain identical which is also confirmed by our analytical expression (27). We would like to mention that, considering the SF network in lower γ ($\gamma < 3$), the theoretical forward point comes closer to the backward point, although a small width of ES is confirmed for a different set of realizations.

Now we will show the impact of multiplexity over frustration. We consider a multiplex network in which ER networks are used on both layers. In earlier literature, synchronization has been examined in two identical networks connected through interlayer links [31]. However, the impact of frustration in identically coupled networks has not been examined. To realize ES, we consider a nonfrustrated environment in layer I where $\alpha = 0$. The change of order parameter (with respect to λ) is shown in Fig. 5(a) with the red line and the blue line shows a continuous transition in layer II due to the presence of strong frustration ($\alpha = 1$). Surprisingly, as the interlayer interactions are switched on, both the layers exhibit ES behavior as shown in Fig. 5(b). Note that the value of the order parameter of layer II (blue color) is enhanced in the multilayer due to the impact of layer I, an interesting phenomenon not discussed previously in a phase-frustrated environment. The dashed vertical lines represent the critical coupling strengths calculated analytically. The backward points are in close agreement with the numerical values; however the forward points have small discrepancy (mainly in multiplex structure) with the numerics. Although, the multiplexity wins over frustration by setting all layers to ES.

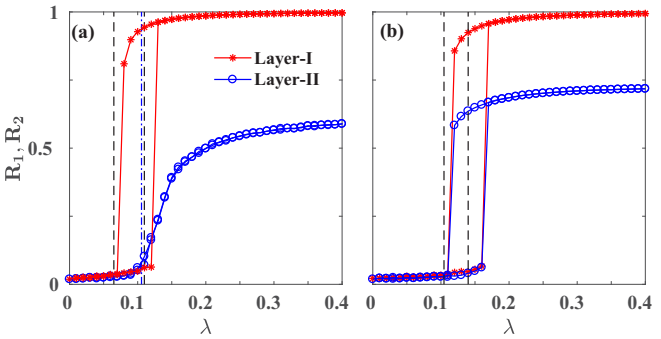

FIG. 5. Order parameters of two layers are shown as a function of λ in the absence (a) and presence (b) of interlayer interactions. Vertical dashed lines represent critical points determined from the self-consistent equations (10) and (11), (12) and (13), and from Eq. (26).

We have also extended our result and verified this feature for SF-SF bilayer networks in which one layer is highly frustrated ($\alpha = 1$) whereas the other layer is not frustrated ($\alpha = 0$). Figure 6(b) shows that (1) ES can be established for both layers if there is layer-layer interaction and (2) the order parameter can be slightly enhanced with an emergence of a short window of explosive synchronization in a multiplex network (shown in blue color).

V. CONCLUSIONS

We found here that a network can impact or affect the sharp transition of a frustrated system. For instance, an SF network in lower γ cannot undergo a first-order transition. On the other hand, for a given network, a strong phase frustration inhibits

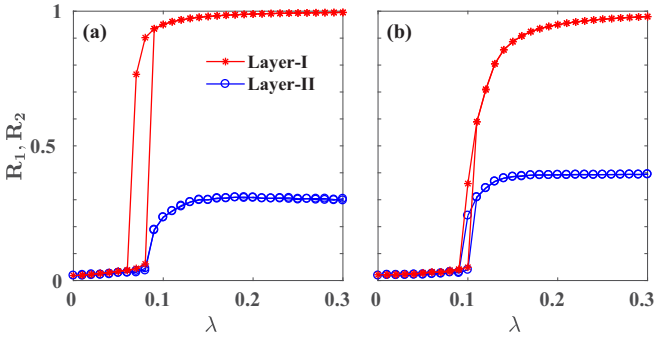

FIG. 6. Panel (a) indicates the order parameter evaluation as a function of λ in the absence of interlayer interaction. The red line shows hysteresis for $\alpha = 0$ in layer I and the blue line shows synchronization pattern of layer II when $\alpha = 1$. There is no ES in layer II. (b) Both of the networks reveal ES (shown by red and blue lines) in the presence of multiplexity in which two layers are connected through adaptive links. Both the layers are equipped with a scale-free network of size $N = 2000$, $\langle k \rangle = 14$, and $\gamma = 3.5$.

ES by promoting a continuous transition to synchronization. We have established that we can transform a continuous transition to a discontinuous transition by feeding them into a multiplex network in which each layer is adaptively controlled by the other layer. We have numerically shown the emergence of ES and our analytical approach predicts the accurate condition of emergence of ES in a multilayer as well as in its monolayer counter part. Using a mean-field analysis and a perturbative approach around the incoherent state, we have calculated the critical coupling strengths for the onset of synchronization both for forward and backward transition. Our approach can easily be extended to other frequency distributions.

ACKNOWLEDGMENTS

P.K. acknowledges support from DST, India, under the Department of Science and Technology, INSPIRE scheme (Code: IF140880). C.H. is supported by Department of Science and Technology, INSPIRE faculty grant (Code: IFA17-PH193).

APPENDIX: DETAILED CALCULATION OF MEAN-FIELD ANALYSIS

The contributions of locked oscillators and drift oscillators to the order parameter are

$$R_l = \frac{(\cos\alpha - i\sin\alpha)}{\langle k\rangle}\int_{k_{min}}^{\infty}\int kP(k)g(\omega)\left[\sqrt{1-\left(\frac{\omega-\Omega}{\lambda rkR}\right)^2}+i\frac{\omega-\Omega}{\lambda rkR}\right]dkd\omega H\left(1-\left|\frac{\omega-\Omega}{\lambda rkR}\right|\right), \tag{A1}$$

$$R_d = \frac{(\sin\alpha + i\cos\alpha)}{\langle k\rangle}\int_{k_{min}}^{\infty}\int P(k)g(\omega)\frac{\omega-\Omega}{\lambda rR}\left[1-\sqrt{1-\left(\frac{\lambda rkR}{\omega-\Omega}\right)^2}\right]dkd\omega H\left(\left|\frac{\omega-\Omega}{\lambda rkR}\right|-1\right). \tag{A2}$$

Hence we get $R = R_l + R_d$, where R_l and R_d are given by Eq. (A1) and Eq. (A2), respectively. Now comparing the real and imaginary parts separately we get the following.

Taking the real part:

$$\begin{aligned} R = &\left(\frac{\cos\alpha}{\langle k\rangle}\int_{k_{min}}^{\infty}\int kP(k)g(\omega)\sqrt{1-\left(\frac{\omega-\Omega}{\lambda rkR}\right)^2}+\frac{\sin\alpha}{\langle k\rangle}\int_{k_{min}}^{\infty}\int kP(k)g(\omega)\frac{\omega-\Omega}{\lambda rkR}\right)H\left(1-\left|\frac{\omega-\Omega}{\lambda rkR}\right|\right)dkd\omega\\ &+\frac{\sin\alpha}{\langle k\rangle}\int_{k_{min}}^{\infty}\int kP(k)g(\omega)\frac{\omega-\Omega}{\lambda rkR}\left[1-\sqrt{1-\left(\frac{\lambda rkR}{\omega-\Omega}\right)^2}\right]H\left(\left|\frac{\omega-\Omega}{\lambda rkR}\right|-1\right)dkd\omega \end{aligned}$$

$$\begin{aligned} \Rightarrow R\langle k\rangle = &\cos\alpha\int_{k_{min}}^{\infty}\int kP(k)g(\omega)\sqrt{1-\left(\frac{\omega-\Omega}{\lambda rkR}\right)^2}H\left(1-\left|\frac{\omega-\Omega}{\lambda rkR}\right|\right)dkd\omega\\ &+\left\{\sin\alpha\int_{k_{min}}^{\infty}\int kP(k)g(\omega)\frac{\omega-\Omega}{\lambda rkR}H\left(1-\left|\frac{\omega-\Omega}{\lambda rkR}\right|\right)+\sin\alpha\int_{k_{min}}^{\infty}\int kP(k)g(\omega)\frac{\omega-\Omega}{\lambda rkR}H\left(\left|\frac{\omega-\Omega}{\lambda rkR}\right|-1\right)\right\}dkd\omega\\ &-\sin\alpha\int_{k_{min}}^{\infty}\int kP(k)g(\omega)\frac{\omega-\Omega}{\lambda rkR}\sqrt{1-\left(\frac{\lambda rkR}{\omega-\Omega}\right)^2}H\left(\left|\frac{\omega-\Omega}{\lambda rkR}\right|-1\right)dkd\omega. \end{aligned} \tag{A3}$$

Taking the imaginary part:

$$\begin{aligned} 0 = &\left(\frac{\cos\alpha}{\langle k\rangle}\int_{k_{min}}^{\infty}\int kP(k)g(\omega)\frac{\omega-\Omega}{\lambda rkR}-\frac{\sin\alpha}{\langle k\rangle}\int_{k_{min}}^{\infty}\int kP(k)g(\omega)\sqrt{1-\left(\frac{\omega-\Omega}{\lambda rkR}\right)^2}\right)H\left(1-\left|\frac{\omega-\Omega}{\lambda rkR}\right|\right)dkd\omega\\ &+\frac{\cos\alpha}{\langle k\rangle}\int_{k_{min}}^{\infty}\int kP(k)g(\omega)\frac{\omega-\Omega}{\lambda rkR}\left[1-\sqrt{1-\left(\frac{\lambda rkR}{\omega-\Omega}\right)^2}\right]H\left(\left|\frac{\omega-\Omega}{\lambda rkR}\right|-1\right)dkd\omega \end{aligned}$$

$$\begin{aligned} \Rightarrow \cos\alpha\int_{k_{min}}^{\infty}\int kP(k)g(\omega)\frac{\omega-\Omega}{\lambda rkR}dkd\omega = &\sin\alpha\int_{k_{min}}^{\infty}\int kP(k)g(\omega)\sqrt{1-\left(\frac{\omega-\Omega}{\lambda rkR}\right)^2}H\left(1-\left|\frac{\omega-\Omega}{\lambda rkR}\right|\right)dkd\omega\\ &+\cos\alpha\int_{k_{min}}^{\infty}\int P(k)g(\omega)(\omega-\Omega)\sqrt{1-\left(\frac{\lambda rkR}{\omega-\Omega}\right)^2}H\left(\left|\frac{\omega-\Omega}{\lambda rkR}\right|-1\right)dkd\omega. \end{aligned} \tag{A4}$$

Now from the above equation of the real part and imaginary part we get coupled equations of the order parameter and group angular frequency in the form given by Eqs. (10) and (11). In the mean-field framework we can take $r_i = R$. To simplify our calculation we introduce a variable $x = \lambda R^2$ and substituting in Eq. (10) and Eq. (11) we obtain three sets of equations for the unknown parameters Ω, R, and x in the following form. Here it is convenient to consider Ω and R as the functions of x:

$$\langle\omega\rangle - \Omega(x) = x\tan\alpha \int_{k_{min}}^{\infty}\int kP(k)g(\omega)\sqrt{1-\left(\frac{\omega-\Omega(x)}{xk}\right)^2}\,H\left(1-\left|\frac{\omega-\Omega}{xk}\right|\right)dkd\omega$$
$$\times \int_{k_{min}}^{\infty}\int p(k)g(\omega)[\omega-\Omega(x)]\sqrt{1-\left(\frac{xk}{\omega-\Omega(x)}\right)^2}\,H\left(\left|\frac{\omega-\Omega}{xk}\right|-1\right)dkd\omega, \tag{A5}$$

$$R^2(x) = \frac{x}{\lambda}, \tag{A6}$$

and

$$R(x)\langle k\rangle = \cos\alpha \int_{k_{min}}^{\infty}\int kP(k)g(\omega)\sqrt{1-\left(\frac{\omega-\Omega}{xk}\right)^2}\,H\left(1-\left|\frac{\omega-\Omega}{xk}\right|\right)dkd\omega + \frac{\sin\alpha}{x}(\langle\omega\rangle-\Omega)$$
$$-\sin\alpha\int_{k_{min}}^{\infty}\int kP(k)g(\omega)\frac{\omega-\Omega}{xk}\sqrt{1-\left(\frac{xk}{\omega-\Omega}\right)^2}\,H\left(\left|\frac{\omega-\Omega}{x}\right|-1\right)dkd\omega. \tag{A7}$$

Solving Eq. (A5) and Eq. (A6) we find x and the group angular frequency Ω. Inserting them into Eq. (A7) we can find the order parameter R.

[1] A. Pikovsky, M. Rosenblum, and J. Kurths, *Synchronization: A Universal Concept in Nonlinear Sciences* (Cambridge University Press, Cambridge, 2003).

[2] S. Boccaletti, J. Kurths, G. Osipov, D. L. Valladares, and C. S. Zhou, Phys. Rep. **366**, 1 (2002).

[3] S. H. Strogatz, *Sync: The Emerging Science of Spontaneous Order* (Hypernion, New York, 2003).

[4] Y. Kuramoto, *Chemical Oscillations, Waves, and Turbulence* (Springer, New York, 1984).

[5] J. A. Acebròn, L. L. Bonilla, C. J. P. Vicente, F. Ritort, and R. Spigler, Rev. Mod. Phys. **77**, 137 (2005).

[6] D. Pazó, Phys. Rev. E **72**, 046211 (2004).

[7] F. A. Rodrigues, T. K. D. M. Peron, P. Ji, and J. Kurths, Phys. Rep. **610**, 1 (2016).

[8] S. Boccaletti, J. A. Almendral, S. Guan, I. Leyva, Z. Liu, I. Sendiña-Nadal, Z. Wan, and Y. Zou, Phys. Rep. **660**, 1 (2016).

[9] J. Gómez-Gardeñes, S. Gomez, A. Arenas, and Y. Moreno, Phys. Rev. Lett. **106**, 128701 (2011).

[10] I. Leyva, A. Navas, I. Sendiña-Nadal, J. A. Almendral, J. M. Buldu, M. Zanin, D. Papo, and S. Boccaletti, Sci. Rep. **3**, 1281 (2013); Y. Zou, T. Pereira, M. Small, Z. Liu, and J. Kurths, Phys. Rev. Lett. **112**, 114102 (2014).

[11] C. Q. Wang, A. Pumir, N. B. Garnier, and Z. Liu, Front. Phys. **12**, 128901 (2017).

[12] U. Lee, M. Kim, K. Lee, C. M. Kaplan, D. Clauw, S. Kim, G. Mashour, and R. Harris, Sci. Rep. **8**, 243 (2018).

[13] P. Kumar, D. K. Verma, P. Parmananda, and S. Boccaletti, Phys. Rev. E **91**, 062909 (2015).

[14] R. S. Pinto and A. Saa, Phys. Rev. E **91**, 022818 (2015).

[15] X. Zhang, X. Hu, J. Kurths, and Z. Liu, Phys. Rev. E **88**, 010802(R) (2013).

[16] I. Leyva, I. Sendiña-Nadal, J. A. Almendral, A. Navas, S. Olmi, and S. Boccaletti, Phys. Rev. E **88**, 042808 (2013).

[17] C. Xu, Y. Sun, J. Gao, T. Qiu, Z. Zheng, and S. Guan, Sci. Rep. **6**, 21926 (2016).

[18] G. Filatrella, N. F. Pedersen, and K. Wiesenfeld, Phys. Rev. E **75**, 017201 (2007).

[19] X. Zhang, S. Boccaletti, S. Guan, and Z. Liu, Phys. Rev. Lett. **114**, 038701 (2015).

[20] M. M. Danziger, O. I. Moskalenko, S. A. Kurkin, X. Zhang, S. Havlin, and S. Boccaletti, Chaos **26**, 065307 (2016).

[21] A. Kachhvah and S. Jalan, Europhys. Lett. **119**, 60005 (2017).

[22] V. Nicosia, P. S. Skardal, A. Arenas, and V. Latora, Phys. Rev. Lett. **118**, 138302 (2017).

[23] M. De Domenico, C. Granell, M. A. Porter, and A. Arenas, Nat. Phys. **12**, 901 (2016).

[24] S. Gómez, A. Díaz-Guilera, J. Gómez-Gardeñes, C. J. Pérez-Vicente, Y. Moreno, and A. Arenas, Phys. Rev. Lett. **110**, 028701 (2013).

[25] H. Sakaguchi and Y. Kuramoto, Prog. Theor. Phys. **76**, 576 (1986).

[26] B. C. Coutinho, A. V. Goltsev, S. N. Dorogovtsev, and J. F. F. Mendes, Phys. Rev. E **87**, 032106 (2013).

[27] T. Ichinomiya, Phys. Rev. E **70**, 026116 (2004).

[28] P. Kundu, P. Khanra, C. R. Hens, and P. Pal, Phys. Rev. E **96**, 052216 (2017); P. Kundu, C. Hens, B. Barzel, and P. Pal, Europhys. Lett. **120**, 40002 (2017).

[29] X. Hu, S. Boccaletti, W. Huang, X. Zhang, Z. Liu, S. Guan, and C. Lai, Sci. Rep. **4**, 7262 (2014); H. Wu, L. Kang, Z. Liu, and M. Dhamala, *ibid.* **8**, 15521 (2018).

[30] J. Aguirre, R. Sevilla-Escoboza, R. Gutiérrez, D. Papo, and J. M. Buldú, Phys. Rev. Lett. **112**, 248701 (2014).

[31] R. Sevilla-Escoboza, I. Sendiña-Nadal, I. Leyva, R. Gutiérrez, J. M. Buldú, and S. Boccaletti, Chaos **26**, 065304 (2016).